

Size effect on fracture properties of concrete after sustained loading

Rong, Hua; Dong, Wei; Zhang, Xue; Zhang, Binsheng

Published in:
Materials and Structures

Publication date:
2019

Document Version
Peer reviewed version

[Link to publication in ResearchOnline](#)

Citation for published version (Harvard):

Rong, H, Dong, W, Zhang, X & Zhang, B 2019, 'Size effect on fracture properties of concrete after sustained loading', *Materials and Structures*, vol. 52, no. 16, pp. 1-12.

General rights

Copyright and moral rights for the publications made accessible in the public portal are retained by the authors and/or other copyright owners and it is a condition of accessing publications that users recognise and abide by the legal requirements associated with these rights.

Take down policy

If you believe that this document breaches copyright please view our takedown policy at <https://edshare.gcu.ac.uk/id/eprint/5179> for details of how to contact us.

Size effect on fracture properties of concrete after sustained loading

Hua Rong¹, Wei Dong^{2,*}, Xue Zhang³, Binsheng Zhang⁴

¹ Senior Engineer, State Key Laboratory of Coastal and Offshore Engineering, Dalian University of Technology, Dalian 116024, P. R. China. & National Test Centre of Quality and Safety Supervision for Industrial Buildings and Structures, Central Research Institute of Building and Construction, MCC, Beijing, 100088, P. R. China. Email: ronghuakeke@163.com

² Professor, State Key Laboratory of Coastal and Offshore Engineering, Dalian University of Technology, Dalian 116024, P. R. China.

*Corresponding author, E-mail: dongwei@dlut.edu.cn

³Lecturer, State Key Laboratory of Coastal and Offshore Engineering, Dalian University of Technology, Dalian 116024, P. R. China. E-mail: xuezhang@dlut.edu.cn

⁴Professor, Department of Civil Engineering and Environmental Management, School of Computing, Engineering and Built Environment, Glasgow Caledonian University, Glasgow G4 0BA, Scotland, United Kingdom. E-mail: Ben.Zhang@gcu.ac.uk

Conflict of interest: The authors declare that they have no conflict of interest.

25 **ABSTRACT**

26 To investigate the size effect on the fracture properties of concrete after sustained loading, concrete
27 beams with three heights of 100 mm, 200 mm and 300 mm were first subjected to 30% peak load
28 over 115 days. Thereafter, they were moved out from the loading frames and tested under standard
29 static three-point bending (TPB) loading until failure. The initial fracture toughness, unstable fracture
30 toughness, fracture energy and evolution of the fracture process zone were then derived based on the
31 experimental results, and the size effect on these fracture properties of concrete after sustained
32 loading were evaluated. The experimental results indicated that compared with the specimens under
33 the static TPB tests without pre-sustained loading, the cracking initiation resistance for the concrete
34 after sustained loading increased, resulting in the increase of the initial cracking load and initial
35 fracture toughness. In particular, the tendency was more significant for the larger size specimens. By
36 contrast, the effects of sustained loading on the unstable fracture toughness, fracture energy, critical
37 crack length and FPZ evolution could be neglected. Furthermore, the size effects on the fracture
38 characteristics, including the fracture energy, and the FPZ evolution were obvious for the concrete
39 specimens both under static loading and after sustained loading.

40

41 Keywords: concrete beam, three-point bending, sustained loading, fracture toughness, fracture
42 energy, size effect

43

44

45

46

47 **Introduction**

48 Delayed failure of concrete structures under sustained loading has a significant effect on the service
49 performance and durability of the structures. Generally, it is considered that linear creep occurs in
50 concrete structures under low load levels, which is caused by viscoelasticity of concrete. By contrast,
51 under high load levels, crack growth interacts with viscoelasticity of the material, resulting in
52 occurrence of nonlinear creep [1]. The crack rate dependence was introduced by Van Zijl et al. [2],
53 which is characterised by the inverse analysis to calculate the time to failure under high sustained
54 loading. The predicted results agreed well with the experimental observations [3]. In fact, creep has
55 two potential effects on the fracture behaviour of concrete structures. Firstly, creep could lead to
56 degradation of structural serviceability, including crack propagation, increase of crack width and
57 deformation. On the other hand, it could decrease the local high stress due to stress re-distribution
58 mechanism in structures [4,5]. Under low sustained loading, there is no crack propagation so that the
59 stress re-distribution at the pre-notch tip governs the variations of fracture properties in concrete. The
60 effects of low sustained loading on the fracture properties at the critical cracking status, such as the
61 critical crack length a_c , the unstable fracture toughness K_{IC}^{un} and the fracture energy G_f , are not clearly
62 clarified. In practice, the size effect on the concrete fracture under sustained loading has attracted
63 attention to academic and engineering communities. According to the research by Barpi and Valente
64 [6], the lifetime of concrete structures appeared to be an increasing function of size, and a critical
65 height of 59 cm was observed. Far from the critical dimension, the size effect on the lifetime
66 appeared to be negligible, as indicated by Bažant and Xiang [7].

67 The fracture parameters, e.g. the fracture toughness and fracture energy, represent the cracking
68 resistance and fracture characteristics of concrete and are generally considered as material properties

69 for fracture analysis. The double- K fracture theory was proposed by Xu and Reinhardt [8, 9] as a
70 modified linear elastic fracture mechanics (LEFM) model to distinguish different cracking stages of
71 concrete, where the fracture process of concrete can be divided into three stages using the initial
72 fracture toughness K_{IC}^{ini} and the unstable fracture toughness K_{IC}^{un} . According to the experimental and
73 theoretical studies under static loading [8-11], these two fracture toughness parameters were
74 size-independent and can be regarded as the material parameters to determine the cracking initiation
75 and unstable propagation in concrete structures. Based on the initial fracture toughness, a crack
76 propagation criterion [12-14] was proposed to determine the crack propagation during the fracture
77 process of concrete. Meanwhile, the effects of loading rate on the double- K fracture parameters were
78 investigated and the results indicated that both K_{IC}^{ini} and K_{IC}^{un} increased with the increased loading
79 rates [15]. In the case of low sustained loading, stress relaxation and re-distribution occur at the crack
80 tip, even though there is no crack propagation at the creep stage. The variations of the stress field at
81 the crack tip would change the cracking resistance of concrete and also affect the initial fracture
82 toughness. However, it is not clarified whether or not the sustained loading affects the crack
83 propagation length and the unstable fracture toughness corresponding to the critical fracture status.

84 Besides fracture toughness, fracture energy is also a significant fracture parameter to characterize the
85 crack propagation resistance of concrete. Previous experimental studies [16-18] showed that the
86 tested fracture energy would increase with the increased specimen size. Accordingly, two theories
87 can be employed to explain the size effect: the size effect law [19] and the boundary effect model
88 [20]. According to the fictitious crack model [21], there exists a fracture process zone (FPZ) ahead of
89 a traction-free crack, where the cohesive stresses are transferred and energy is dissipated. Therefore,
90 fracture energy is directly related to the FPZ, so that the size effect on fracture energy would be

91 involved in the FPZ evolution. Based on the research by Wu et al. [22], the FPZ would increase
92 linearly until the full length was reached, and then decrease when the crack tip approached to the
93 surface of the specimen. Meanwhile, the ratio of the crack length a to the specimen depth D ,
94 corresponding to the full FPZ length, would decrease with the increased specimen size [23].
95 Accordingly, the size effect of the fracture energy could also be reflected when determining the
96 tension-softening constitutive law of concrete [24, 25]. Under sustained loading conditions, based on
97 the researches by Omar et al. [26] and Carpinteri et al. [27], the values of fracture energy under
98 sustained loading and static loading were similar. However, Saliba [28, 29] indicated that, due to the
99 consolidation of hardened cement paste, concrete could be strengthened under sustained loading so
100 that the measured fracture energy and strength slightly increased after sustained loading.

101 **Research significance**

102 The investigations from different researchers indicate that it still remains controversial whether the
103 fracture energy is affected by sustained loading or not. Meanwhile, it is not clarified whether the size
104 effect on the fracture energy of concrete under sustained loading exists. In addition, there are no
105 reports on the size effect on the double- K fracture parameters under sustained loading. Therefore, to
106 assess the cracking stability of concrete structures, it is essentially important to carry out further
107 investigations on the size effect on the fracture properties under sustained loading to obtain a
108 comprehensive understanding of the fracture mechanism of concrete structures in service. Hence, the
109 aim of this paper was to investigate the effects of specimen size on the fracture properties of concrete
110 after low sustained loading. The TPB specimens with the depths of 100 mm, 200 mm and 300 mm
111 were subjected to 30% of the peak load for 115 days. Thereafter, the standard TPB tests were
112 conducted on these specimens. In comparison with the experimental results under static loading, the

113 effects of sustained loading on the fracture properties of the concrete specimens with different sizes
114 were evaluated.

115 **Experimental program**

116 *Specimen preparations*

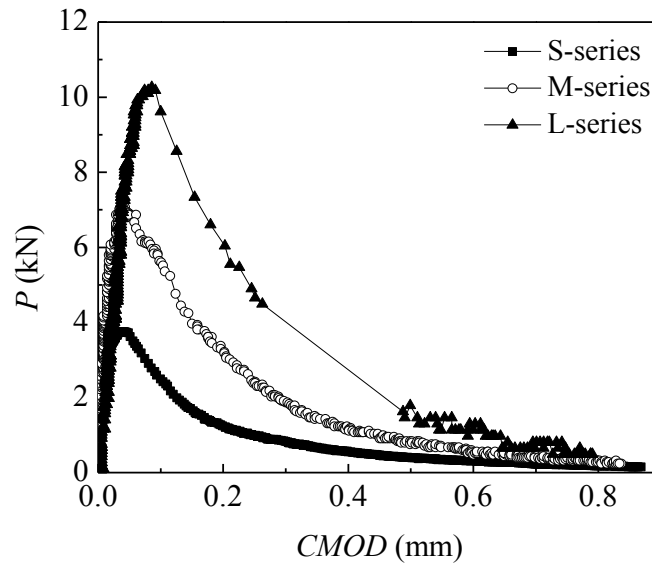
117 To investigate the size effect on the fracture properties of concrete, three series of TPB specimens
118 with similar geometries were measured in this study. The beam heights were 100 mm, 200 mm and
119 300 mm, respectively, with the ratio of the initial notch length to the depth, a_0/D , as 0.3 and the ratio
120 of the depth to the spans as 0.25. The effect of the width was not considered here, so that the width of
121 all specimens was chosen as 100 mm and the distance from the support to the edge of the specimen
122 was chosen as 50 mm. In this study, the specimen sizes were adopted as length \times width \times depth ($L \times$
123 $B \times D$) = 500 mm \times 100 mm \times 100 mm, 900 mm \times 100 mm \times 200 mm and 1300 mm \times 100 mm \times
124 300 mm, respectively. After demolding, all the beam specimens were polished mechanically until the
125 designed sizes were achieved. Thereafter, the beam specimens were processed by using a diamond
126 saw to form the initial notch with the wide of 2 mm and the length of 30% of the beam height. The
127 mix proportions of the concrete were 1 : 0.60 : 2.01 : 3.74 (cement : water : sand : aggregate) by
128 weight and the maximum coarse aggregate size was 10 mm. The specimens were demoulded 24
129 hours after casting and then stored in the standard curing room with 23° and 90% relative humidity
130 for three months to avoid the effects of the autogenous shrinkage at early age and the increased
131 strength on the experimental investigations. The experimental data (Exp.) of the mechanical
132 properties including the elastic modulus E , the splitting tensile strength f_t , and the uniaxial
133 compressive strength f_c at the ages of 28 and 90 days are listed in Table 1. In addition, their statistical
134 results including the average values (Av.) and the standard deviations (S.D.) are calculated

135 accordingly. It can be seen that the standard deviations of the experimental data in Table 1 are
 136 relatively small compared with the average values and the calculated average values show the
 137 coincident tendency, i.e. the mechanical properties of concrete at the age of 90 days are slightly
 138 larger than those at the age of 28 days. Meanwhile, comparing these material properties between the
 139 ages of 90 and 205 days shows that there are no significant variations observed. This indicates that
 140 the mechanical properties of concrete fairly kept constant after the 90-day curing.

141 **Table 1** Mechanical properties of concrete

Age (days)	E (GPa)					f_t (MPa)					f_c (MPa)				
	Exp.1	Exp.2	Exp.3	Av.	S.D.	Exp.1	Exp.2	Exp.3	Av.	S.D.	Exp.1	Exp.2	Exp.3	Av.	S.D.
28	31.9	32.1	34.7	32.9	1.28	2.0	2.3	2.3	2.2	0.14	36.8	38.6	36.2	37.2	1.02
90	36.2	35.8	37.2	36.4	0.59	2.6	2.5	2.4	2.5	0.08	45.9	47.2	45.8	46.3	0.64
205	35.8	33.6	33.5	34.3	1.06	2.7	2.4	2.4	2.5	0.14	44.8	47.5	45.1	45.8	1.21

142
 143 In addition, to calibrate the applied load in the followed creep tests, the standard TPB tests were
 144 conducted on concrete specimens with three sizes at the age of 90 days. For each series, three
 145 specimens were prepared and the average results of the P - $CMOD$ curves for S-, M- and L-series are
 146 shown in Fig 1. The average values of the peak load P_{max} were determined as 3.81 kN, 7.01 kN and
 147 10.34 kN, respectively, which were used to pre-set P_{max} on the creep specimens with the same
 148 geometry. Meanwhile, three more specimens for each condition were cast at the same time and kept
 149 under the same curing conditions without being loaded, named as “aging specimens”. The specimens
 150 with depths of 100 mm, 200 mm and 300 mm were denoted as S-, M- and L-series. For example,
 151 “M-30-1” denotes the TPB beam specimen 1 with sizes of 900 mm \times 100 mm \times 200 mm under the
 152 30% P_{max} loading level.



153
154 **Fig. 1.** *P-CMOD* curves for TPB specimens with different sizes
155

156 ***Creep tests***

157 The basic creep tests under TPB loading were performed first. In order to ensure only the basic creep
158 to be measured in the tests, a double-layer aluminium tape was used to seal all the surfaces of the
159 specimens to prevent the moisture dissipation. It has been proved that the use of a double-layer
160 aluminum tape to seal the specimens can effectively prevent the dissipation of the interior moisture
161 from the specimen surface [1]. Also, this method is adopted by the American Association of State
162 Highway and Transportation Officials (i.e. AASHTO PP34-99: Standard Practice for Cracking
163 Tendency Using a Ring Specimen) and American Society for Testing Material (i.e. the ASTM
164 C1581/C1581M-09a: Standard Test Method for Determining Age at Cracking and Induced Tensile
165 Stress Characteristics of Mortar and Concrete under Restrained Shrinkage) to assess the cracking
166 tendency of concrete under restrained shrinkage. Meanwhile, the steel loading frames with different
167 sizes were designed for performing the creep tests. Fig.2 illustrates the typical set-up for Specimen
168 S-30-1 under the creep test. The load cell was put between the frame and the specimen and
169 connected to a bolt, and the load was applied by turning the bolt. For the S-, M- and L series
170 specimens subjected to $30\%P_{max}$, the bolts were turned until the load levels of 1.14 kN, 2.10 kN and

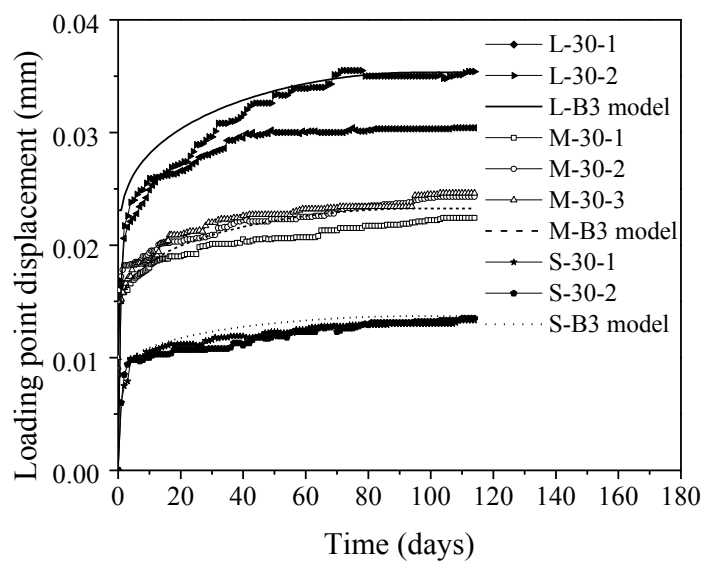
171 3.10 were reached, respectively. The data acquisition system with a digital display was used to record
172 the real-time load readings. The loading point displacement (δ) and CMOD were measured using the
173 dial gauges (see Fig. 2). The creep tests were conducted inside an environmental chamber with 23°
174 and 60% relative humidity. During the creep tests, the loads would be increased to the pre-set values
175 if they decreased by 2%. The loading duration for the creep tests was 115 days, and the mechanical
176 properties of concrete at the age of 205 days (90 + 115 days) are also listed in Table 1.



177
178 **Fig. 2.** Set-up for Specimen S-30-1 under the creep test

179 Fig. 3 illustrates the loading point displacement versus time curves ($\delta - t$ curves) for the S-, M- and
180 L-series specimens. It can be seen that the creep deformation increased with the increased specimen
181 size. For each size specimen, the creep deformation increased significantly in the first 10 days of
182 loading, and then the increase became slow until an approximate stable status was reached two
183 months after the loading. As shown in Fig. 2, the mechanical dial gauges were used to measure the
184 loading point displacements during the creep tests, whose measurement resolution is 1 micrometer.
185 From Fig. 3, it can be seen that the variations of the loading point displacements could be detected
186 for both the rapid growth stage at early age and the stabilization stage at later age. Therefore, this
187 resolution of 1 micrometer would allow for accurate measurements of the loading point
188 displacements during the creep tests. It should be noted that, due to the effect of the measurement

189 resolution of the device, the displacement variations could not be monitored when the deflected
190 values were smaller than 1 micrometer. Meanwhile, the B3 model [30] was utilised to predict the
191 creep deformation over time for the S-, M- and L-series specimens. The predicted results showed
192 reasonably good agreements with the experimental data, which indicates that the B3 model is
193 appropriate for assessing the creep deformation of concrete specimens with different sizes under low
194 sustained loading.

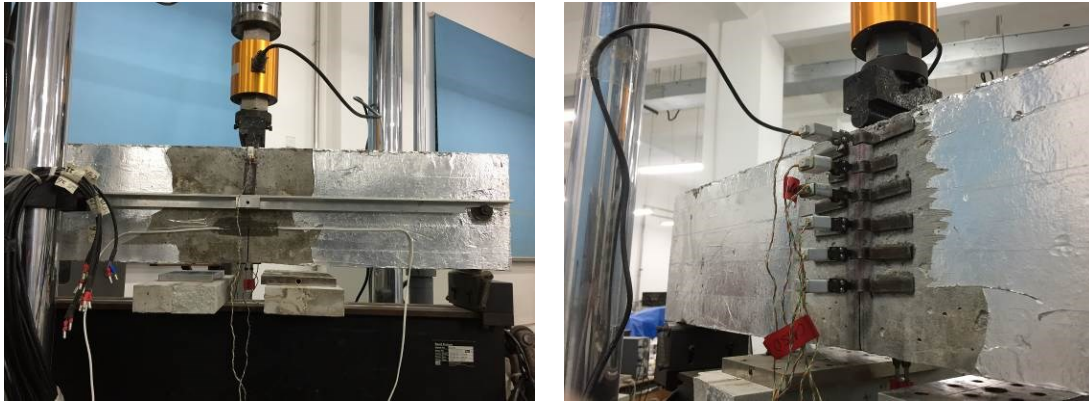


195
196
197

Fig. 3. Loading point displacement versus time curves in the creep tests

198 *Standard TPB tests*

199 After 115 days of sustained loading, the specimens in the creep tests were moved out from the
200 loading frames and then immediately tested under the standard TPB loading. A 250 kN closed loop
201 servo-controlled MTS testing machine was used for loading the TPB beams, including the creep and
202 aging specimens prepared in this study, at a displacement rate of 0.048 mm/min. A clip gauge was
203 mounted on the bottom of each beam to measure the *CMOD* during loading. In order to obtain the
204 crack propagation length, the clip gauges were placed equidistantly along the ligament length to
205 measure the crack opening displacements. The experimental set-up for the standard TPB tests and the
206 arrangements of the clip gauges are illustrated in Figs. 4(a) and (b), respectively.



208

209 (a) Measuring loading point displacement and *CMOD* (b) Measuring crack opening displacement

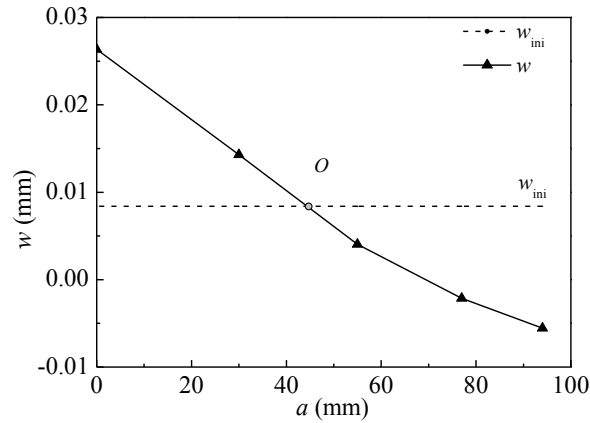
210

211

Fig. 4. Experimental set-up for the standard TPB tests

212 The displacement at the crack initiation, w_{ini} , could be calibrated by measuring the crack tip opening
 213 displacement (*CTOD*) with respect to the initial cracking load on the aging specimen. According to
 214 the research by Xu et al. [8], the crack tip opening displacement (*CTOD*) at the crack initiation can
 215 be regarded to be size-independent. Therefore, the average displacement at the crack initiation, w_{ini} ,
 216 determined from the S-series TPB specimens as 8.423×10^{-6} m, was used to characterize the crack
 217 initiation for all the S-, M- and L-series specimens. To measure the initial cracking load, four strain
 218 gauges were symmetrically pasted on both sides of the specimen surface, 5 mm away from the tip of
 219 the pre-notch. Once a new crack began to initiate, the measured strains from the strain gauges would
 220 drop rapidly due to the sudden release of the stored strain energy at the tip of the pre-crack. Based on
 221 the measured *CMODs* and crack opening displacements (w) at the different positions along the
 222 ligament, an approximately linear distribution of the crack opening displacements was obtained.
 223 Taking Specimen S-30-1 as an example, the crack opening displacements approximately linearly
 224 distributed along the crack surface, as shown in Fig. 5. Furthermore, by comparing w_{ini} and w , the
 225 crack tip can be determined, which is marked as Point “O” in Fig. 5. Accordingly, the crack
 226 propagation lengths with respect to various loading points could also be obtained from the positions
 227 of the derived crack tip during the complete fracture process. By introducing the tension-softening

228 constitutive law of concrete, the FPZ evolution in the crack propagation process could be derived.



229

230

Fig. 5. Determination of the crack tip using clip gauges

231 **Results and discussion**

232 *Effects of sustained loading on the fracture properties*

233 According to the creep deformations illustrated in Fig. 3, the initial cracks did not propagate in the
234 creep tests because the stable displacements for the specimens were observed. For some concrete
235 structures, the load capacity could increase after a low sustained loading, e.g. the variations of the
236 water level for the gravity dams. Therefore, the cracking resistance of concrete structures after a
237 sustained loading is of concern to engineering and academic fields. Based on the sudden drop of the
238 strain around the initial crack tip, the values of the initial cracking load P_{ini} for different specimen
239 sizes were determined from the standard TPB tests, as shown in Table 2. Taking Specimen
240 M-aging-1 as an example, Fig. 6 illustrates the strain variations at the pre-notch tip, where Points A
241 and B correspond to the initial and peak loads, respectively. Compared with the aging specimens,
242 Table 2 indicates that the initial cracking load increased for the specimens subjected to pre-sustained
243 loading. Meanwhile, the increase is more significant for the specimens with larger sizes. For the S-,
244 M- and L-series specimens, the growths in P_{ini} were 7.5%, 54.2% and 62.7%, respectively. By

245 contrast, the effect of sustained loading on the peak load is not significant, compared with the aging
 246 specimens, the changes in P_{\max} being -1.95%, 18.23% and 11.17% for the S-, M- and L-series
 247 specimens, respectively.

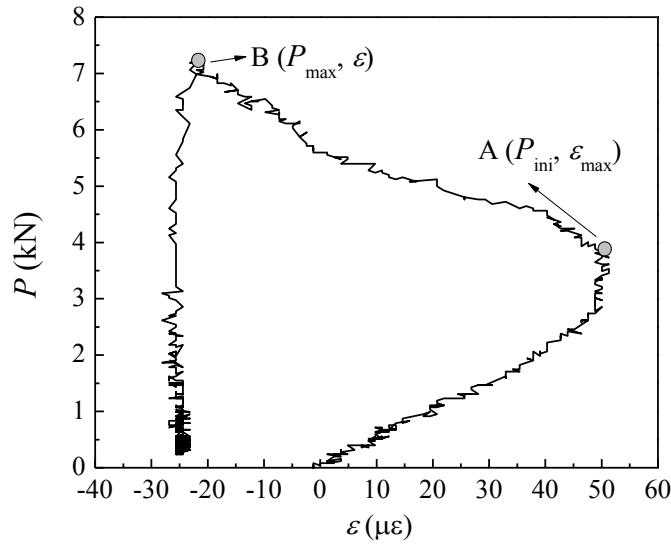
248

Table 2. Experimental results for the TPB tests

Specimens	P_{ini} (kN)	P_{max} (kN)	a_c (mm)		$K_{\text{IC}}^{\text{ini}}$ (MPa·m ^{1/2})	$K_{\text{IC}}^{\text{un}}$ (MPa·m ^{1/2})	G_f (N/m)	L_{ch} (mm)	
			Cal.	Exp.					
S-aging-1	2.66	3.56	52.08	55.15	0.51	1.42	81.71	464.02	
S-aging-2	2.53	3.68	48.10	50.63	0.49	1.27	102.22	580.50	
S-aging-3	2.51	3.61	49.13	50.25	0.49	1.22	87.43	496.51	
Mean	2.55	3.59	49.77	52.01	0.50	1.28	90.45	513.66	
S.D.	0.07	0.05	1.69	2.23	0.01	0.08	8.64	49.07	
C.I.	Lower	2.49	3.56	47.75	49.34	0.49	1.20	80.11	454.91
	Upper	2.62	3.68	51.79	54.68	0.51	1.41	100.80	572.44
S-30-1	2.88	3.79	50.98	52.78	0.55	1.31	88.64	503.38	
S-30-2	2.61	3.25	54.36	54.90	0.50	1.29	85.64	486.34	
Mean	2.74	3.52	52.67	53.84	0.53	1.30	87.14	494.86	
S.D.	0.135	0.27	1.69	1.06	0.03	0.01	1.5	8.52	
C.I.	Lower	2.55	3.12	50.19	52.29	0.49	1.29	84.94	482.37
	Upper	2.94	3.92	55.15	55.39	0.56	1.31	89.34	507.35
M-aging-1	4.13	6.76	79.72	83.66	0.56	1.19	97.07	551.25	
M-aging-2	4.14	7.40	87.60	91.23	0.56	1.46	100.98	573.45	
M-aging-3	4.46	6.70	79.54	86.51	0.61	1.18	88.22	500.99	
Mean	4.24	6.95	82.29	87.13	0.58	1.28	95.42	541.88	
S.D.	0.15	0.32	3.76	3.12	0.02	0.13	5.34	30.31	
C.I.	Lower	4.06	6.57	77.79	83.40	0.55	1.12	89.03	505.60
	Upper	4.43	7.33	86.79	90.87	0.60	1.43	101.81	578.19
M-30-1	6.59	8.53	76.78	80.17	0.90	1.45	90.62	514.62	
M-30-2	7.11	8.77	81.31	86.68	0.97	1.58	102.96	584.70	
M-30-3	5.93	8.21	82.14	89.87	0.81	1.50	90.12	511.78	
Mean	6.54	8.50	80.08	85.57	0.89	1.51	94.57	537.05	
S.D.	0.48	0.23	2.36	4.04	0.06	0.05	5.94	33.73	
C.I.	Lower	5.97	8.23	77.26	80.74	0.81	1.45	87.46	496.65
	Upper	7.12	8.78	82.90	90.41	0.97	1.57	101.68	577.41
L-aging-1	4.54	9.00	128.17	134.40	0.54	1.40	132.53	752.62	
L-aging-2	4.99	9.98	127.76	129.67	0.55	1.55	141.63	804.30	
Mean	4.77	9.49	131.63	132.04	0.55	1.47	137.08	778.46	
S.D.	0.23	0.49	0.21	2.37	0.01	0.075	4.55	25.84	
C.I.	Lower	4.44	8.77	127.66	128.57	0.54	1.37	130.41	740.57
	Upper	5.09	10.21	128.27	135.50	0.55	1.58	143.75	816.35
L-30-1	7.39	9.65	126.90	127.54	0.82	1.49	146.81	833.72	

L-30-2	8.14	10.46	130.93	136.02	0.90	1.68	147.63	838.37	
Mean	7.76	10.06	128.28	131.78	0.86	1.59	147.22	836.05	
S.D.	0.38	0.41	2.02	4.24	0.04	0.10	0.41	2.33	
C.I.	Lower	7.22	9.46	125.96	125.56	0.80	1.45	146.62	832.64
	Upper	8.31	10.64	131.87	138.00	0.92	1.72	147.82	839.45

249



250

251

Fig. 6. Strain variations at the pre-notch tip of Specimen M-aging-1

252

The values of the critical crack length a_c obtained from the experimental measurements and

253

analytical method [9] are also included in Table 2. The equation for analytically calculating a_c is

254

given as follows:

255

$$a_c = \frac{2}{\pi} (D + H_0) \arctan \sqrt{\frac{B \cdot E \cdot CMOD_c}{3 \cdot 2 \cdot P_{max}}} \quad 0.11E \quad (1)$$

256

where $CMOD_c$ is the critical crack mouth opening displacement measured in the tests, and H_0 is the

257

thickness of the knife edge and is equal to 3 mm in this study.

258

The values of a_c in Table 2 indicate that the analytical and experimental results are in a reasonably

259

good agreement, and confirm that the analytical equation from LFM is appropriate for determining

260

the critical crack length after low sustained loading. After obtaining the peak loads and the critical

261

crack propagation lengths from the tests, the initial and unstable fracture toughnesses, K_{IC}^{ini} and K_{IC}^{un} ,

262 can be calculated [9] as

$$263 \quad K_{IC}^{ini} = \frac{3P_{ini}S}{2D^2B} \sqrt{a_0} F_2 \left(\frac{a_0}{D} \right) \quad (2)$$

$$264 \quad K_{IC}^{un} = \frac{3P_{max}S}{2D^2B} \sqrt{a_c} F_2 \left(\frac{a_c}{D} \right) \quad (3)$$

265
266 where S is the span of the specimens and $F_2 \left(\frac{a}{D} \right)$ can be calculated from the following equation:

$$267 \quad F_2 \left(\frac{a}{D} \right) = \frac{1.99 - \left(\frac{a}{D} \right) \left(1 - \frac{a}{D} \right) \left[2.15 - 3.93 \left(\frac{a}{D} \right) + 2.7 \left(\frac{a}{D} \right)^2 \right]}{\left(1 + 2 \frac{a}{D} \right) \left(1 - \frac{a}{D} \right)^{3/2}} \quad (4)$$

268 Noted that a in Eq. (4) should be substituted by a_0 and a_c for the solution of K_{IC}^{ini} and K_{IC}^{un} , respectively.

269 The values of K_{IC}^{ini} and K_{IC}^{un} for all specimens are listed in Table 2. It can be seen that there are no

270 significant size effects on the two fracture toughnesses obtained under static loading, which confirms

271 the finding obtained by Xu et al. [8]. However, the scenarios are different for the specimens with

272 various sizes after sustained loading. Compared with the aging specimens, the values of K_{IC}^{ini} for the

273 S-, M- and L-serials specimens after sustained loading increased by 6.0%, 53.5% and 56.4%,

274 respectively. With the increased specimen size, the initial fracture toughness was significantly

275 enhanced. By contrast, the effect of the specimen size on the unstable fracture toughness K_{IC}^{un} was not

276 prominent, with net increases of 1.6%, 18%, and 0.8% for the S-, M- and L-serials specimens only.

277 It should be noted that the double- K theory [9] was employed in the analyses, so that the variation

278 tendencies for K_{IC}^{ini} and K_{IC}^{un} matched those for P_{ini} and P_{max} . Comparing the measured and calculated

279 values of a_c indicates that the double- K theory is fairly appropriate for determining the fracture

280 properties of concrete at the critical status after low sustained loading. Accordingly, K_{IC}^{un} is a fracture

281 parameter governing the crack unstable propagation. Thus, the calculated K_{IC}^{un} using the double- K
282 theory would be available if considering the negligible effect of low sustained loading. However, K_{IC}^{ini}
283 is a fracture parameter governing the resistance on the crack initiation. Even under a low sustained
284 loading, the stress re-distribution would occur at the tip of the pre-notch and this cannot be reflected
285 in the analyses based on the double- K theory. Consequently, in the case of K_{IC}^{ini} , the double- K theory
286 may be not appropriate, i.e. the calculated results of K_{IC}^{ini} may not be convincing. The work
287 considering the effect of stress re-distribution at the tip of the pre-notch will be conducted in the
288 further study.

289 Besides the initial and unstable fracture toughnesses, the fracture energy G_f is also an important
290 fracture parameter for concrete, which is defined as the required energy for creating the cracking area
291 and can be calculated using the following equation recommended by RILEM [31] as:

$$292 \quad G_f = \frac{W_f}{A_{lig}} = \frac{W_0 + mg\delta_0}{B(D - a_0)} \quad (5)$$

293 where W_f is the total absorbed energy, A_{lig} is the ligament area, W_0 is the area under the measured
294 load-deformation curve, mg is the self-weight of the specimen, and δ_0 is the loading-point
295 displacement at failure.

296 The obtained values of G_f are listed in Table 2. With the increased specimen size, the values of G_f
297 increased under the static loading, and this can be explained by the models for the size and boundary
298 effects [19, 20]. Compared with the results under static loading, the fracture energy was not affected
299 by low sustained loading but increased with the increased specimen sizes.

300 To verify the reliability of the conclusions on the size effect of fracture properties, the standard
301 deviations (S.D.) and the confidence intervals (C.I.) with a confidence level of 95% are calculated
302 for all the configurations, which are listed in Table 2. It can be seen from the table that the standard

303 deviations are relatively small, i.e. less than 10% of the corresponding average values for all the
 304 configurations. In addition, by comparing the confidence intervals (the lowers or the uppers) between
 305 different configurations, the conclusions on the size effect of fracture properties can also be obtained,
 306 which agree well with those obtained based on only the average values.

307

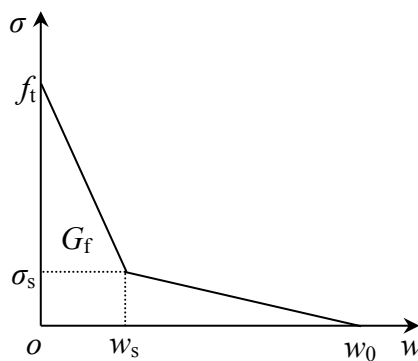
308 ***Effects of sustained loading on the FPZ evolution***

309 According to the measuring method introduced in this study, the crack propagation lengths and the
 310 opening displacements with respect to various loading stages can be determined using clip gauges.

311 Furthermore, a tension softening constitutive law was introduced to characterise the relationship
 312 between the crack opening displacement w and the cohesive stress σ . According to the fictitious

313 crack model [21], the nonlinear softening characteristics of the FPZ in concrete can be described
 314 using the σ - w relationship, where the stress-free crack opening displacement w_0 governs the FPZ

315 ending. Thus, the FPZ length can be determined as the distance from the crack tip to the position of
 316 stress-free crack. In this study, the bilinear σ - w relationship was adopted, as illustrated in Fig. 7.



317

318 **Fig. 7.** Bilinear σ - w concrete softening curve

319 According to Petersson [32], the parameters σ_s , w_s and w_0 in this figure can be determined as:

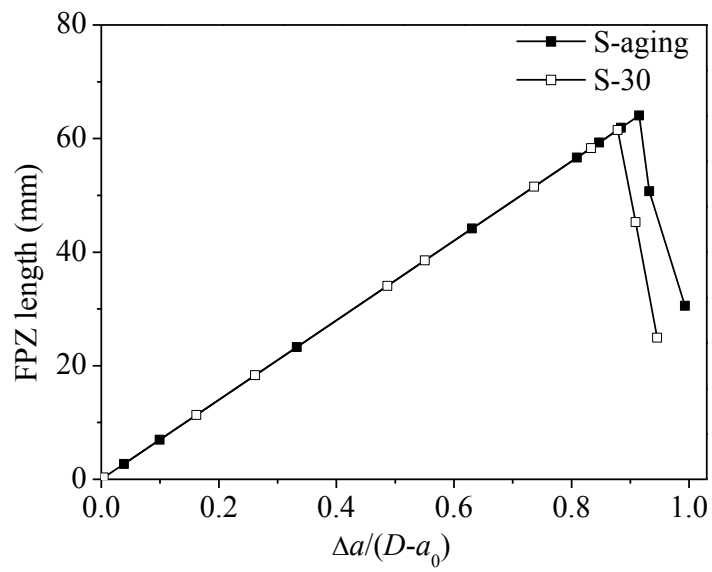
320

$$\sigma_s = f_t / 3 \quad (6)$$

321
$$w_s = 0.8G_f/f_t \quad (7)$$

322
$$w_0 = 3.6G_f/f_t \quad (8)$$

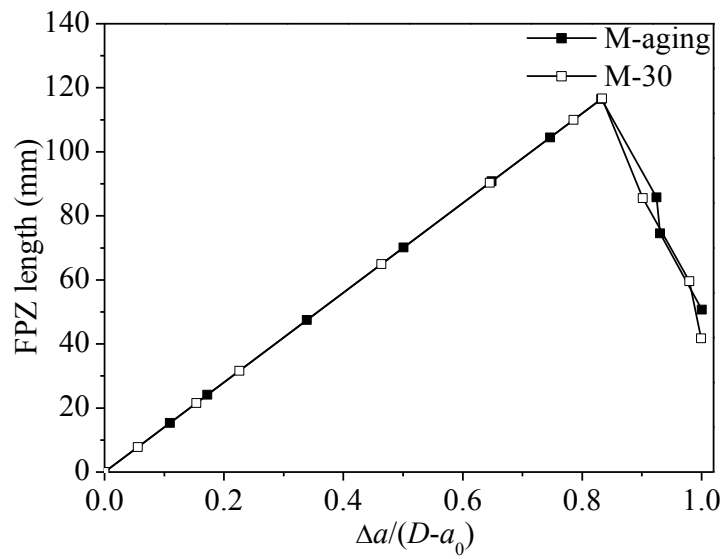
323 where w_s and σ_s are the crack opening displacement and the cohesive stress at the break-point of the
324 bilinear $\sigma-w$ relationship. According to the experimental results of G_f and f_t , the bilinear $\sigma-w$
325 relationship can be determined, which could be employed to quantify the FPZ length during the
326 loading process. Figs. 8 (a) to (c) illustrate the FPZ evolution for the S-, M- and L-series specimens,
327 respectively. For a vibrant comparison between the static and creep loading conditions, the average
328 curve was used for each loading condition. From Fig. 8, it can be seen that for each specimen size,
329 the FPZ length increased linearly with the crack propagation, and then decreased after reaching a full
330 evolution of the FPZ. The values of $\Delta a/(D-a_0)$ for the full FPZ length of the S-aging-, M-aging- and
331 L-aging-series specimens were 0.89, 0.83 and 0.77, respectively. Accordingly, the full FPZ lengths
332 for the three series specimens were determined as 61.5 mm, 116.7 mm and 161.4 mm. Although the
333 ratio of $\Delta a/(D-a_0)$ decreased due to the boundary effect for the larger specimens, the full FPZ length
334 still increased with the increased specimen size. Hence, the crack propagation in larger size
335 specimens needs to overcome more resistance caused by the cohesive characteristics of concrete,
336 resulting in the enhancement of fracture energy. Comparing with the aging specimens indicates that
337 the FPZ evolution for the creep specimens showed similar variation trends. Thus, it can be seen that
338 the effects of low sustained loading on the fracture energy and the FPZ evolution could be neglected,
339 while the size effects still exist for the concrete after low sustained loading. Moreover, vertical cracks
340 formed along the ligament length for all S-, M- and L-series specimens under TPB loading. To show
341 the final crack patterns of the TPB specimens, the patterns for the S-creep specimens, as an example,
342 have been illustrated in Fig. 9.



343

344

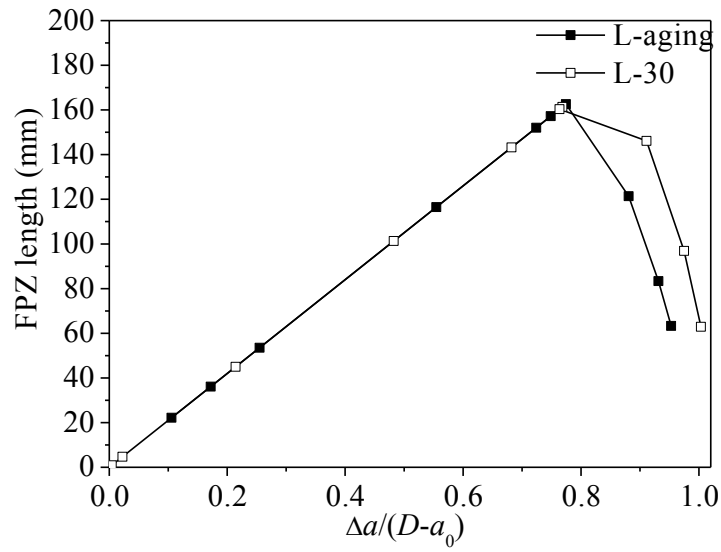
(a) S-series specimens



345

346

(b) M-series specimens



347

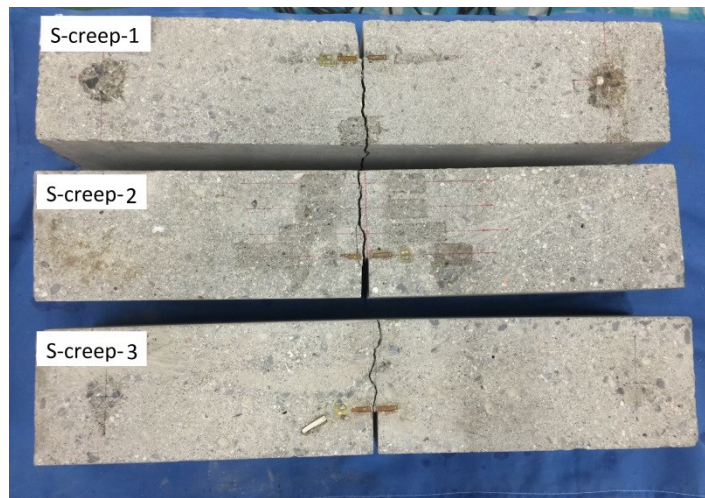
348

(c) L-series specimens

349

Fig. 8. FPZ evolutions for the S-, M-, and L-series specimens

350



351

352

Fig. 9. Final crack patterns of the S-creep specimens

353 The characteristic length L_{ch} in mm was used to quantify the brittleness of the concrete specimens

354 and is defined as

355

$$L_{ch} = \frac{EG_F}{f_t^2} \quad (9)$$

356 A small characteristic length indicates a larger brittleness of the material. The results of L_{ch} are listed
357 in Table 2. It can be seen that the values of L_{ch} increased with the increased specimen size. For the
358 aging specimens with the depths of 100 mm, 200 mm and 300 mm, the mean values of L_{ch} were
359 obtained as 513.66 mm, 541.88 mm and 778.46 mm, respectively. Comparatively, for the creep
360 specimens, the mean values were obtained as 494.86 mm, 537.05 mm and 836.05 mm, respectively.
361 Although the value of L_{ch} was significantly affected by the specimen size, the effects of low
362 sustained loading on L_{ch} can be reasonably ignored. Accordingly, under higher sustained loading, the
363 brittleness of concrete has been found to increase by Omar et al. [26] if the size effect law is
364 introduced [33].

365 **Conclusions**

366 The concrete specimens with three sizes were prepared to investigate the size effect on the fracture
367 properties of concrete after sustained loading. The creep tests were conducted on the TPB specimens
368 by applying a sustained load of 30% P_{max} over 115 days. Thereafter, the standard TPB tests were
369 conducted to measure the initial cracking load, the peak load, the critical crack propagation length
370 and the fracture energy, and the FPZ evolution during the fracture process was determined from the
371 experimental results. By comparing the results of the concrete specimens under static loading with
372 those after sustained loading, the following conclusions can be drawn:

373 (a) Low sustained loading had a significant effect on the crack initiation, resulting in the increase of
374 the initial cracking load and initial fracture toughness. Also, with the increased specimen size, the
375 initial fracture toughness increased, showing significant variations compared with the results
376 under static loading. However, it should be noted that the derivation of the initial fracture
377 toughness was still based on the LEFM theory and the stress re-distributions were not considered

378 in the analyses.

379 (b) Comparing the experimental and analytical results indicates that the peak load, the critical crack
380 length and the unstable fracture toughness were not affected by the applied sustained loading,
381 while the unstable fracture toughness was still size-independent. Therefore, the calculated
382 method based on the double- K theory is still appropriate for determining the fracture parameters
383 of concrete at the critical fracture status under low sustained loading.

384 (c) Under the applied low sustained loading, the fracture energy appeared to be size dependent,
385 which is similar to the case under static loading. Meanwhile, the FPZ evolution was affected by
386 the boundary of the specimen and its full length increased with the increasing specimen size, due
387 to the size effect on the fracture energy. In general, the crack initiation was significantly affected
388 by low sustained loading, while this effect can be neglected for the complete crack propagation
389 and the unstable fracture analysis because of no crack propagation at this stage.

390

391 **Acknowledgements**

392 The authors gratefully acknowledge the financial support of the National Natural Science Foundation
393 of China under the grants NSFC 51878117, NSFC 51421064 and NSFC 51708565, the Fundamental
394 Research Funds for the Central Universities of China under the grant DUT17LK06, and the National
395 Basic Research Program of China (The 973 Program) under the grant 2015CB057703.

396 **References**

- 397 1. Saliba J, Loukili A, Grondin F, Regoin JP (2014) Identification of damage mechanisms in
398 concrete under high level creep by the acoustic emission technique. *Mater Struct* 47
399 (6):1041-1053.
- 400 2. Van Zijl GPAG, De Borst R and Rots JG (2001) The role of crack rate dependence in the
401 long-term behaviour of cementitious materials. *Int J Solids Struct* 38 (30-31):5063-5079.

- 402 3. Zhou FP (1992) Time-dependent crack growth and fracture in concrete. Dissertation, Lund
403 University, Sweden.
- 404 4. Beushausen H, Masuku C, Moyo P (2012) Relaxation characteristics of cement mortar
405 subjected to tensile strain. *Mater Struct* 45 (8):1181-1188.
- 406 5. Hamed E (2016) Relaxation behavior of concrete under sustained uniaxial compressive
407 deformation. *J Mater Civil Eng* 28 (6): 06016007(06016001-06016007)
- 408 6. Barpi F, Valente S (2011) Failure lifetime of concrete structures under creep and fracture.
409 *Mag Concr Res* 63 (5):371-376.
- 410 7. Bažant ZP, Xian YY (1997) Crack growth and lifetime of concrete under long time loading. *J*
411 *Eng Mech - ASCE* 123 (4):350-358.
- 412 8. Xu S, Reinhardt HW (1999) Determination of double-K criterion for crack propagation in
413 quasi-brittle fracture: Part I Experimental investigation of crack propagation. *Int J Fract* 98
414 (2):111-149.
- 415 9. Xu S, Reinhardt HW (1999) Determination of double-K criterion for crack propagation in
416 quasi-brittle fracture: Part II Analytical evaluating and practical measuring methods for
417 three-point bending notched beams. *Int J Fract* 98 (2):151-177.
- 418 10. Bruhwiler E, Wittmann FH (1990) The wedge splitting test, a new method of performing
419 stable fracture-mechanics tests. *Eng Fract Mech* 35 (1-3):117-125.
- 420 11. Qing L, Dong M, Guan J (2018) Determining initial fracture toughness of concrete for
421 split-tension specimens based on the extreme theory. *Eng Fract Mech* 189:427-438.
- 422 12. Dong W, Wu Z, Zhou X (2013) Calculating crack extension resistance of concrete based on a
423 new crack propagation criterion. *Constr Build Mater* 38 (1):879-889.
- 424 13. Wu Z, Wu X, Dong W, Zheng J, Wu Y (2014) An analytical method for determining the crack
425 extension resistance curve of concrete. *Mag Concr Res* 66 (14):719-728.
- 426 14. Dong W, Wu Z, Tang X, Zhou X (2018) A comparative study on stress intensity factor-based
427 criteria for the prediction of mixed mode I-II crack propagation in concrete. *Eng Fract Mech*
428 197:217-235.
- 429 15. Hu S, Zhang X, Xu S (2015) Effects of loading rates on concrete double-K fracture
430 parameters. *Eng Fract Mech* 149:58-73.
- 431 16. Wittmann FH, Mihashi H, Nomura N (1990) Size effect on fracture energy of concrete. *Eng*
432 *Fract Mech* 35 (1-3):107-115.
- 433 17. Zhao Z, Kwon SH, Shah SP (2008) Effect of specimen size on fracture energy and softening
434 curve of concrete: Part I Experiments and fracture energy. *Cem Concr Res* 38
435 (8-9):1049-1060.
- 436 18. Guan JF, Li QB, Wu ZM, Zhao SB, Dong W, Zhou SW (2016) Fracture parameters of
437 site-cast dam and sieved concrete. *Mag Concr Res* 68 (1):43-54.
- 438 19. Hoover CG, Bažant ZP (2014) Comparison of the Hu-Duan boundary effect model with the
439 size-shape effect law for quasi-brittle fracture based on new comprehensive fracture tests. *J*
440 *Eng Mech* 140 (3):480-486.
- 441 20. Hu XZ, Guan JF, Wang YS, Keating A, Yang ST (2017) Comparison of boundary and size
442 effect models based on new developments. *Eng Fract Mech* 175:146-167.
- 443 21. Hillerborg A, Modéer M, Petersson PE (1976) Analysis of crack formation and crack growth
444 in concrete by means of fracture mechanics and finite elements. *Cem Concr Res* 6
445 (6):773-781.

- 446 22. Wu Z, Rong H, Zheng J, Xu F, Dong W (2011) An experimental investigation on the FPZ
447 properties in concrete using digital image correlation technique. *Eng Fract Mech* 78
448 (17):2978-2990.
- 449 23. Dong W, Zhou X, Wu Z (2013) On fracture process zone and crack extension resistance of
450 concrete based on initial fracture toughness. *Constr Build Mater* 49 (12):352-363.
- 451 24. Kwon SH, Zhao Z, Shah SP (2008) Effect of specimen size on fracture energy and softening
452 curve of concrete: Part II Inverse analysis and softening curve. *Cem Concr Res* 38
453 (8-9):1061-1069.
- 454 25. Murthy AR, Karihaloo BL, Iyer NR, Prasad BKR (2013) Bilinear tension softening diagrams
455 of concrete mixes corresponding to their size-independent specific fracture energy. *Constr*
456 *Build Mater* 47:1160-1166.
- 457 26. Omar M, Loukili A, Pijaudier-Cabot G, Pape YL (2009) Creep-damage coupled effects:
458 Experimental investigation on bending beams with various sizes. *J Mater Civil Eng* 21
459 (2):65-72.
- 460 27. Carpinteri A, Valente S, Zhou F, Ferrara G, Melchiorri G (1997) Tensile and flexural creep
461 rupture tests on partially-damaged concrete specimens. *Mater Struct* 30 (5):269-276.
- 462 28. Saliba J, Grondin F, Loukili A, Regoin J Coupling creep and damage in concrete under high
463 sustained loading. In: *Proceedings of the 7th International Conference in Fracture Mechanics*
464 *of Concrete and Concrete Structures*, Jeju, Korea, 2010.
- 465 29. Saliba J, Loukili A, Grondin F, Regoin J (2012) Experimental study of creep-damage
466 coupling in concrete by acoustic emission technique. *Mater Struct* 45 (9):1389-1401.
- 467 30. Bažant ZP, Baweja S, RILEM Committee TC 107-1, ACI Committee 209-2 (1995) Creep and
468 shrinkage prediction model for analysis and design of concrete structures - Model B3. *Mater*
469 *Struct* 28 (180):357-365.
- 470 31. RILEM TCS 50 (1985) Rilem TC 50-FMC recommendation: Determination of the fracture
471 energy of mortar and concrete by means of three-point bend tests on notched beams. *Mater*
472 *Struct* 18 (4):287-290.
- 473 32. Petersson PE (1981) Crack growth and development of fracture zones in plain concrete and
474 similar materials. Report TVBM-1006, Division of Building Materials, Lund Institute of
475 Technology, Sweden, 1981.
- 476 33. Bažant ZP (1984) Size effect in blunt fracture: concrete, rock, metal. *J Eng Mech* 110
477 (4):518-535.